Research Square

Preprints are preliminary reports that have not undergone peer review.
They should not be considered conclusive, used to inform clinical practice,
or referenced by the media as validated information.

Green Synthesis and Physicochemical Characterization of Biogenic Silver Nanoparticles for Comparative Sunlight and Uv Photocatalytic Degradation of Congo Red

Aditya s
Sathyabama Institute of Science and Technology
Vimal A
Sathyabama Institute of Science and Technology
Kavipraba A
Kavipraba.a.bte@sathyabama.ac.in

Sathyabama Institute of Science and Technology

Research Article

Keywords: Bacillus subtilis AVK-21, Congo Red degradation, Green synthesis, Photocatalytic dye degradation, Silver nanoparticles

Posted Date: February 26th, 2026

DOI: https://doi.org/10.21203/rs.3.rs-8757702/v1

License: This work is licensed under a Creative Commons Attribution 4.0 International License.
Read Full License

Additional Declarations: No competing interests reported.

Version of Record: A version of this preprint was published at Nanotechnology for Environmental Engineering on May 21st, 2026. See the published version at https://doi.org/10.1007/s41204-026-00561-w.

GREEN SYNTHESIS AND PHYSICOCHEMICAL CHARACTERIZATION OF BIOGENIC SILVER NANOPARTICLES FOR COMPARATIVE SUNLIGHT AND UV PHOTOCATALYTIC DEGRADATION OF CONGO RED

ABSTRACT

Silver nanoparticles (Ag NPs) were biosynthesized using *Bacillus subtilis* AVK-21 isolated from water samples, wherein microbial metabolites served as natural reducing and stabilizing agents for the reduction of Ag^{+} to Ag^{0} nanoparticles. The formation of Ag NPs was confirmed by a distinct SPR peak observed in UV-Vis spectroscopy at 430 nm, while FTIR analysis revealed functional biomolecules responsible for nanoparticle capping. SAED pattern depicts the crystalline face-centered cubic structure of the particles, and energy-dispersive X-ray spectroscopy (EDS) verified elemental silver with energy peak near 3keV. Transmission electron microscopy (TEM) demonstrated predominantly spherical nanoparticles with an average primary size of 62.4 nm, whereas dynamic light scattering (DLS) indicated a hydrodynamic diameter of 271.3 nm, reflecting the aggregation behavior of the biogenic Ag NPs. The zeta potential value was found to be 0.0 mV which further supported their limited colloidal stability and corresponded with the clustered morphology seen in TEM micrographs. The photocatalytic efficiency of the biosynthesized Ag NPs was evaluated using Congo Red dye under two conditions i.e., sunlight and UV light in which sunlight exposure resulted in significantly greater degradation (67.01%) compared to UV irradiation (37.80%) within 120 min. The enhanced effectiveness under sunlight is attributed to stronger plasmonic excitation and improved ROS generation, which facilitated electron transfer and the subsequent breakdown of the dye's structure. Overall, this study demonstrates that microbially synthesized Ag NPs possess good photocatalytic potential and can efficiently degrade Congo Red under natural sunlight, highlighting their applicability as sustainable, low-energy catalysts for dye-polluted wastewater treatment.

Keywords: *Bacillus subtilis* AVK-21, Congo Red degradation, Green synthesis, Photocatalytic dye degradation, Silver nanoparticles

Article Highlights

- Water-derived *Bacillus subtilis* produces stable silver nanoparticles sustainably.
- Ag NP nanoparticles efficiently break down Congo Red dye under sunlight.
- Study provides insights for sustainable wastewater treatment applications.

LIST OF ABBREVIATIONS

Ag	Silver
AgNO3	Silver nitrate
Ag NPs	Silver Nanoparticles
BLAST	Basic Local Alignment Search Tool
CH-Ag NPs	Chemically Synthesized Silver Nanoparticles
DLS	Dynamic Light Scattering
EDS	Energy Dispersive X-ray Spectroscopy
FTIR	Fourier-Transform Infrared Spectroscopy
HCl	Hydrochloric Acid
ITS	Internal Transcribed Spacer
mV	Millivolt
NaOH	Sodium Hydroxide
PDI	Polydispersity Index
ppm	Parts per million
ROS	Reactive Oxygen Species
rpm	Revolution per minute
rRNA	Ribosomal Ribonucleic Acid
SAED	Selected Area Electron Diffraction
SPR	Surface Plasmon Resonance
UV-Vis	Ultraviolet-Visible Spectroscopy

1. INTRODUCTION

Water pollution from dyes is a major environmental concern, especially in industrial areas where untreated waste is often discharged into water bodies. The textile industry alone accounts for 20% of global wastewater pollution, releasing large quantities of toxic, non-biodegradable dyes into the environment. Azo dyes, in particular, are widely used for their vibrant colors and stability, but they pose serious ecological and health risks. Some common examples include Tartrazine (E102), a yellow dye used in beverages and confectionery, and Sunset Yellow (E110), an orange dye used in snacks and baked goods [1]. Congo red, a commonly used azo dye in textile and paper industries, is highly persistent in the environment due to its complex aromatic structure, which makes it resistant to biodegradation and conventional wastewater treatment [2]. Its accumulation in water bodies reduces light penetration, impairs photosynthesis, and disrupts aquatic ecosystems. Under anaerobic conditions, Congo red can degrade into aromatic amines, many of which are mutagenic and carcinogenic, posing significant risks to human health [3]. Long-term exposure can lead to skin irritation, respiratory issues, liver toxicity, and potential carcinogenic effects, while its bioaccumulation in aquatic organisms can magnify toxicity along the food chain [4-6]. These properties make Congo red a major concern for environmental safety and public health, highlighting the urgent need for efficient and eco-friendly removal strategies. It is estimated that 2,00,000 tons of Congo Red is discharged into the environment annually, with concentrations in textile effluent reaching up to 500 parts per million (ppm) [7]. Conventional methods for dye removal, such as adsorption and photocatalysis, can be expensive and energy-intensive [8]. Consequently, researchers are exploring alternative solutions, and Ag NPs have emerged as a promising candidate for dye degradation due to their unique properties.

Ag NPs possess unique physicochemical properties that enable their application across diverse fields [9]. They have been extensively utilized in environmental remediation, where their high surface area and reactivity facilitate the degradation of pollutants and microbial contaminants in water systems. They are also employed in catalysis, supporting reduction and oxidation reactions, and in electronics, due to their excellent conductivity for use in conductive inks and printed electronic devices. Their optical properties, particularly surface plasmon resonance, make them valuable for biosensing and diagnostic applications, allowing sensitive detection of biomolecules. Furthermore, the antimicrobial activity of Ag NPs is harnessed in medical applications, including coatings for medical devices, disinfectants, and drug delivery systems, highlighting their versatile role in both therapeutic and preventive applications [10].

Conventional chemical and physical methods for synthesizing silver nanoparticles, such as chemical reduction, photochemical synthesis, and solvothermal processes, can be effective in producing nanoparticles for various applications. However, they often require toxic reducing agents (e.g., sodium borohydride, hydrazine), generate hazardous by-products, and demand high energy input, which raises environmental and safety concerns [11]. In contrast, microbial synthesis offers a green, sustainable alternative. Microorganisms, including bacteria, fungi, and

algae, use naturally occurring biomolecules as reducing and stabilizing agents, enabling nanoparticle formation under mild conditions without harmful chemicals. This approach is eco-friendly, cost-effective, and biocompatible, and it allows some control over nanoparticle size and shape, making microbial synthesis a safer and more sustainable method for producing Ag NPs compared to conventional chemical approaches [12-17]. Microorganisms, such as bacteria, fungi, and algae, have the ability to reduce silver ions (Ag^{+}) to metallic silver, leading to the formation of Ag NPs with diverse morphologies [18-25].

Research has indicated that green synthesized Ag NPs can efficiently degrade a variety of dyes. Previous studies have reported that the catalytic activity of Ag NPs for dye degradation can depend on factors such as nanoparticle size, type of dye, and synthesis method [26]. Ag NPs synthesized using plant extracts, such as *Citrus reticulata* peel and *Amaranthus gangeticus Linn (Chinese spinach) leaf extract*, have been reported to degrade malachite green and Congo Red, respectively, under sunlight irradiation [27,28]. Green synthesized Ag NPs have also been reported to degrade a variety of other dyes, including 4-nitrophenol [29], as well as mixtures of dyes found in industrial wastewater [30]. In addition, bacterial species such as *Micrococcus luteus*, *Klebsiella pneumoniae*, and *Enterobacter aerogenes* have been employed to synthesize Ag NPs capable of degrading methyl orange [30]. Certain Bacillus species are particularly effective in Ag NP biosynthesis due to their metabolic versatility and secretion of reducing and stabilizing biomolecules. For instance, *Bacillus subtilis* has been reported to produce spherical Ag NPs via extracellular metabolites [31], while *Bacillus licheniformis* and *Bacillus cereus* have also been utilized to generate Ag NPs capable of catalytically degrading methylene blue [32]. Microalgae and fungi, notably *Fusarium oxysporum*, have been employed to biosynthesize Ag NPs capable of degrading dyes such as Methyl Red and Crystal Violet [33]. Although previous studies have demonstrated the potential of microbe-mediated Ag NP synthesis, systematic investigations addressing the degradation of persistent dyes, such as Congo red, are still limited. While plant-based (particularly leaf-extract) methods dominate green synthesis, microbial approaches offer distinct advantages, including eco-friendliness, biocompatibility, and the ability to control nanoparticle size and morphology. To address this gap, the present study investigates microbial synthesis of Ag NPs and evaluates their efficacy for sustainable and eco-friendly dye remediation.

2. MATERIALS AND METHODOLOGY

2.1 MATERIALS

Silver nitrate ($AgNO_3$) was purchased from Merck Millipore, India. Sodium hydroxide (NaOH, analytical grade), and hydrochloric acid (HCl, analytical grade), nutrient agar and nutrient broth were procured from SRL Chemicals, India. Distilled water was used for all solution preparations. Nutrient agar and nutrient broth were used for microbial cultivation. Laboratory equipment included a cooling centrifuge (Microfuge 20R, Beckman Coulter, USA), magnetic stirrer (IKA C-MAG HS 7 magnetic stirrer ,Germany), Laminar hood, and sterilized glassware (flasks, beakers, micropipettes). All reagents and glassware were sterilized before use following Standard Methods (APHA, 2017) [34].

2.2 WATER SAMPLE COLLECTION

Water samples were collected following ISO 19458:2006 guidelines for microbiological water sampling and APHA Standard Methods (2017) for preservation and transport. Samples were aseptically obtained from four low-human-activity sites in Madurai—Mudalaikulam 1 (9.988904° N, 77.937628° E), Mudalaikulam 2 (9.988845° N, 77.937685° E), Sholavandhan (10.007563° N, 77.971474° E), and the Vaigai River (9.349986° N, 79.0700° E)—using pre-sterilized 200 mL plastic containers. Water was collected from a depth of 20–30 cm to avoid surface contamination. Containers were labelled, placed in ice-cooled insulated carriers, transported to the laboratory, and stored at 4°C, with processing completed within 24 hours to maintain microbial viability.

2.3 ISOLATION OF MICROBES USING SPREAD PLATE METHOD

The water sample bottle was vigorously shaken to homogenize the microbial population. Serial dilutions were performed by transferring 1 mL of the sample into 9 mL of sterile distilled water. Successive dilutions (10^{-1} to 10^{-4}) were prepared to achieve a suitable concentration for plating. Using a sterile micropipette, 0.1 mL of the desired dilution was transferred onto the surface of the solidified agar in a petri dish. The sample was spread evenly over the agar surface using a sterile glass spreader or L-shaped rod [35]. After the incubation period of 24-48 h at 37°C, microbial growth was observed on the nutrient agar plates inoculated with water samples. Distinct microbial colonies were observed on the four sample plates, exhibiting variations in size, shape, color, and texture as shown in figure S1 (Online Resource).

2.4 STREAKING FOR PURE CULTURES

After incubation, spread plates were examined for isolated colonies based on distinct characteristics such as size, color, shape, texture, and edge definition, and six colonies were selected from four sample plates. The inoculating loop was sterilized by flame, allowed to cool, and then used to gently pick a colony, which was streaked onto a fresh nutrient agar plate in a zigzag pattern across four quadrants to reduce the microbial load and isolate individual colonies, ensuring minimal overlap [36]. The streaked plates were inverted and incubated at 37°C for 24–48 h, resulting in well-separated colonies with no contamination as shown in Fig 1.

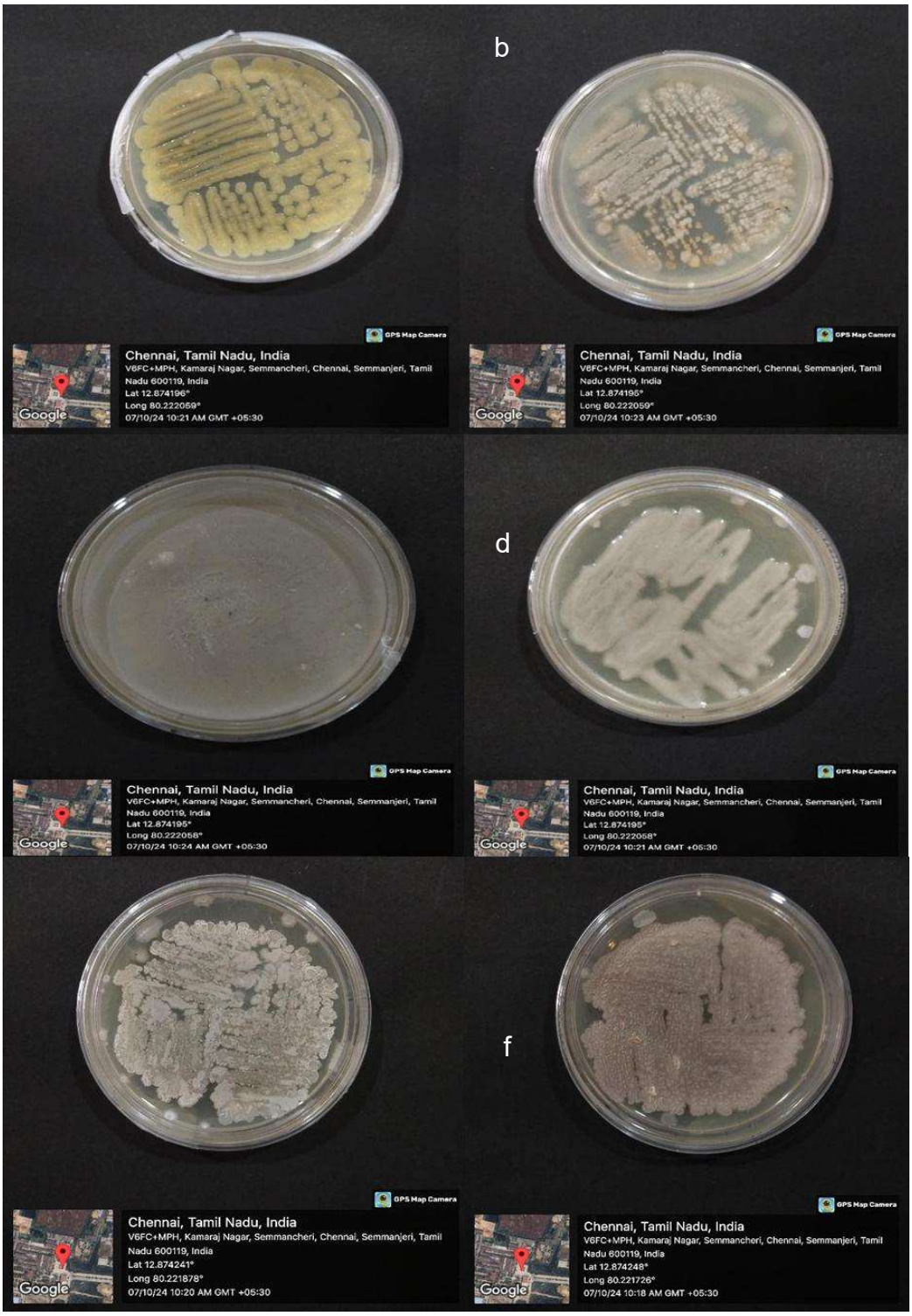


Fig.1 Streak plates of six microbial isolates used for Ag NP biosynthesis. Panels (a–f) correspond to isolates 1 through 6, respectively. Each plate shows the characteristic colony morphology of the respective isolate

2.5 PREPARATION OF BROTH CULTURE

Sterile nutrient broth was prepared by dissolving the required amount of powdered medium in distilled water (e.g., 13 g/L), and autoclaved at 121°C for 15 min to ensure sterility. A single isolated colony from the streak plate was selected using a sterile loop and inoculated into a sterile 100 mL conical flask containing 100 mL of nutrient broth under aseptic conditions for each of the six samples. The inoculated flasks were incubated at 37°C in a shaker incubator at 120-150 rpm for 18–24 h to promote uniform growth. After incubation, visible turbidity was observed in all six flasks, indicating microbial growth as shown in figure S2 (Online Resource). No contamination was detected.

2.6 STAINING

Two types of staining were performed: Simple Staining and Gram Staining. Simple staining, using Methylene Blue that identifies bacterial cells by enhancing contrast, making cell features like shape, size, and arrangement easier to observe under a microscope. Gram Staining categorizes bacteria into Gram-positive (purple) and Gram-negative (pink/red) based on their cell wall structure.

For simple staining, a smear was prepared on a clean slide with a drop of sterile water and a loopful of broth culture, which was air-dried and heat-fixed. Methylene blue was applied for 1-2 min, excess stain was washed off, and the slide was air-dried [37]. Under a microscope at 100x magnification, all six samples were examined and found to be bacteria. Streaks 1, 2, and 5 exhibited cocci-shaped cells; Streaks 3 and 4 showed rod-shaped bacteria; and Streak 6 displayed round cells resembling cocci as shown in figure S3 (Online Resource).

For Gram staining, a smear was prepared in the same manner, followed by crystal violet for 1 min, Gram's iodine for 1 min, ethanol for 15-30 s, and Safranin for 1 minute [37]. The slide was examined under a microscope at 100x magnification with immersion oil, and the results were recorded: Gram-positive bacteria appeared purple, and Gram-negative bacteria appeared pink. All six samples were examined, and among the six isolates, three were observed to be Gram-positive (appearing purple) i.e., Streak 3, Streak 5 and Streak 6, while three were Gram-negative (appearing pink) i.e., Streak 1, Streak 2 and Streak 4.

2.7 MICROBIAL IDENTIFICATION BY SEQUENCING

Microbial sequencing is a precise method used to identify and characterize microorganisms by analyzing their genetic material. It helps distinguish species by targeting specific genes, such as the 16S rRNA gene for bacteria and archaea [38]. The sequencing method used for the identification was Sanger sequencing.

Out of 6 isolates, a single isolate was considered for the sequencing and further synthesis of Ag NPs. Streak 4 was selected for sequencing as it was having morphologically distinctive characteristics with mucoidal appearance. 16S rRNA was used for the identification of the bacteria. For this purpose, the pure culture of the isolate was submitted to a commercial sequencing service provider, NGS Hub, National Facility for Coastal and Marine Research, Sathyabama

Institute of Science and Technology, Chennai, India. The entire sequencing workflow, including genomic DNA extraction, PCR amplification, and sequencing, was carried out by the consultancy.

Genomic DNA was extracted from the bacterial sample using a standard phenol-chloroform method or a commercially available DNA extraction kit, as per the consultancy's protocol. The 16S rRNA gene was then amplified using universal bacterial primers (such as 27F and 1492R), targeting conserved regions of the gene. The amplified products were purified and subjected to Sanger sequencing using cycle sequencing chemistry with fluorescently labeled dideoxynucleotides.

The resulting chromatogram files were analyzed for base calling and sequence quality. The final consensus sequence was compared against the NCBI GenBank database using the BLAST algorithm to identify the isolate based on sequence homology with known bacterial strains. The bacterial species showing the highest similarity percentage and alignment score was considered as the identified strain. The identified strain was subsequently used for the biosynthesis of silver nanoparticles.

2.8 BIOSYNTHESIS OF AG NPS

Ag NPs were synthesized microbially, where biologically active molecules reduced Ag^{+} to Ag^{0}. Enzymes such as nitrate reductase, along with proteins and polysaccharides, served as both reducing and stabilizing agents, while their functional groups provided surface capping to prevent aggregation and ensure colloidal stability. [39]. For the synthesis, a selected bacterial species was cultured in nutrient broth at 37°C and the optical density of the bacterial culture was measured to be 0.57 which indicates the log phase of the bacteria, after which the culture was centrifuged at 12000 rpm for 10 min to separate the biomass from the supernatant. The obtained supernatant was then added to 1 mM silver nitrate solution in 1:1 volume ratio and incubated at room temperature to facilitate nanoparticle formation as shown in figure S5 (Online Resource) [40]. The synthesized nanoparticles were purified by centrifugation at 15000xg for 15 min multiple times and washed with deionized water to eliminate unreacted ions and biomolecular residues [41]. Finally, the purified Ag NPs were resuspended in distilled water as shown in figure S6 (Online Resource) and stored at 4°C in dark containers to preserve their stability and prevent light-induced degradation. The workflow is shown in figure 2.

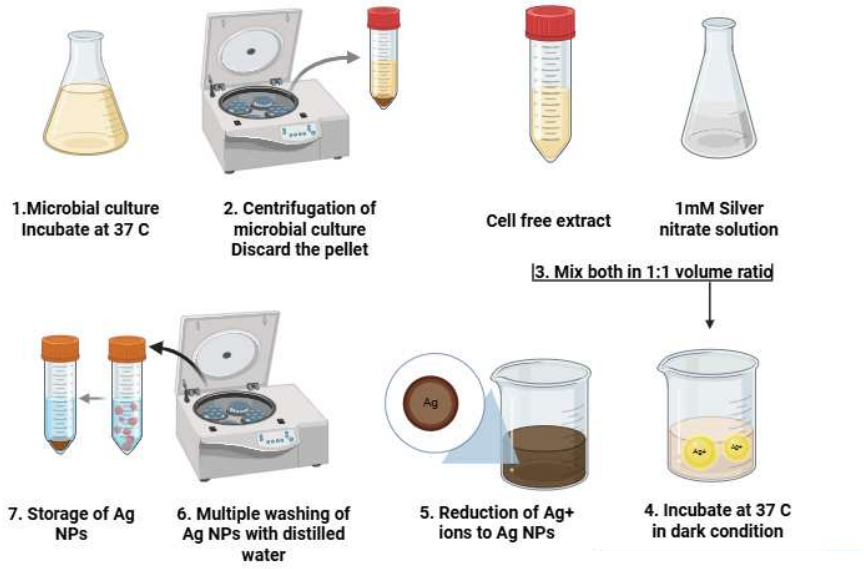


Fig.2 Workflow depicting biosynthesis of nanoparticles

2.9 CHARACTERIZATION OF AG NPS

The synthesized Ag NPs were characterized using various analytical techniques to confirm their formation, stability, and physicochemical properties. SPR peak detection was performed using a Shimadzu UV-1800 UV-visible spectrophotometer (Japan) equipped with a deuterium and tungsten lamp (4000 K) at manufacturer-specified intensity. Absorbance was measured over 200–800 nm, serving as a key indicator of nanoparticle synthesis. [41]. Dynamic light scattering (DLS) was used to determine the average hydrodynamic diameter, polydispersity index (PDI), and colloidal stability of the nanoparticles, while zeta potential analysis was performed to evaluate surface charge and dispersion stability, all carried out on a Horiba nanopartica SZ100V2 (Japan) at the Centre for Ocean Research, Sathyabama Institute of Science and Technology, Chennai, India. FTIR was used to identify functional groups responsible for the reduction and capping of nanoparticles, indicating the involvement of microbial biomolecules using Nicolet Summit-X FTIR spectrometer (Thermo Fisher Scientific, USA) at IIT-M, Chennai [42]. Finally, TEM-EDS was done using Talos F200S G2 TEM (Thermo Fisher Scientific, USA) at Advanced Characterization Facility, Sathyabama Institute of Science and Technology, Chennai which provided high-resolution images to assess the shape, size, and dispersion of the nanoparticles [39], confirming their nanoscale morphology along with the analysis of elemental composition.

2.10 PHOTOCATALYTIC REMEDIATION OF DYE (CONGO RED) USING SILVER NANOPARTICLES

The photocatalytic potential of biosynthesized Ag NPs was assessed through the degradation of Congo Red dye, a commonly used azo dye in our laboratory. To begin, a stock dye solution was prepared by dissolving 100 mg of Congo Red in 1 liter of deionized water, yielding a concentration of 100 mg/L. From this stock, a working solution of 25

mg/L was obtained by diluting 25 mL of the stock with 75 mL of deionized water. For the degradation experiment, 1 mg of Ag NPs was added to 100 mL of the working dye solution in a clean beaker [43]. The mixture was stirred at 200–300 rpm using a magnetic stirrer to ensure homogeneous dispersion of the nanoparticles. The solution's pH was brought within the range of 3 and 7, depending on the requirement, as pH significantly influences photocatalytic efficiency.

The dye-nanoparticle mixture was then exposed to two different light conditions to assess photocatalytic activity: natural sunlight during peak daylight hours and ultraviolet (UV) light at wavelengths such as 254 nm or 365 nm, provided by a UV chamber. In addition to the test samples, control experiments were performed. These conditions allowed for the evaluation of both sunlight- and UV-induced degradation pathways. At specific time intervals- 0, 10, 20, 30, 60, and 120 min, 2 mL aliquots of the reaction mixture were withdrawn to monitor the progress of dye degradation. Each sample was centrifuged at 10,000 rpm for 5 min to remove residual nanoparticles, and the supernatant was analyzed.

The degradation of Congo Red was tracked using UV-Visible spectrophotometry by measuring absorbance at 497 nm, which corresponds to the dye's maximum absorbance wavelength (λ_{max}) [44]. The initial absorbance (A_0) and absorbance at each time interval (A_t) were recorded and compared to determine the percentage of dye degraded over time. The following formula was used to determine the degradation efficiency [45]:

Degradation Efficiency (%) =

$$\frac{(A0 - At)}{A0} \times 100$$

These values were computed for both sunlight and UV exposure conditions, and the results were plotted to provide a comparative understanding of photocatalytic efficiency under different lighting scenarios. This approach highlights the effectiveness of Ag NPs in environmental remediation through dye degradation.

2.11STATISTICAL ANALYSIS

Nanoparticle characterization techniques, including TEM, DLS, zeta potential, and FTIR, were descriptive, as these analyses provide direct instrument-based outputs rather than measurements from independent experimental groups. Photocatalytic dye degradation experiments were monitored over time by measuring absorbance at 497 nm. Each measurement was performed in triplicate, and the mean values were calculated and reported, ensuring accurate and reliable representation of the degradation kinetics. As no comparisons between independent experimental groups were made, inferential statistical tests such as t-tests or ANOVA were not applied.

3. RESULTS AND DISCUSSION

3.1 16S rRNA sequencing confirms the isolate as *Bacillus sp.*

Microbial identification was performed using 16S rRNA gene sequencing. The amplified 16S rRNA sequence as shown in figure 3 was compared against the NCBI GenBank database using BLASTn. The isolate exhibited 96.09% identity with *Bacillus subtilis* strain CICC10076 with Accession number AY917141.1, confirming its taxonomic assignment as shown in figure 4.

SIST3105_CO1 CONTIG:

>SIST3105
TATCTGCAAGTCGAGCGGACAGATGGGAGCTTGCTCCCTGATGTTAGCGGCGGACGGGTGAGTAACACGTGGGTA
ACCTGCCTGTAAGACTGGGATAACTCCGGGAAACCGGGGCTAATACCGGATGGTTGTTTGAACCGCATGGTTCAA
ACATAAAAGGTGGCTTCGGCTACCACTTACAGATGGACCCGCGGCGCATTAGCTAGTTGGTGAGGTAACGGCTCA
CCAAGGCAACGATGCGTAGCCGACCTGAGAGGGTGATCGGCCACACTGGGACTGAGACACGGCCCAGACTCCTAC
GGGAGGCAGCAGTAGGGAATCTTCCGCAATGGACGAAAGTCTGACGGAGCAACGCCGCGTGAGTGATGAAGGTTT
TCGGATCGTAAAGCTCTGTTGTTAGGGAAGAACAAGTACCGTTCGAATAGGGCGGTACCTTGACGGTACCTAACC
AGAAAGCCACGGCTAACTACGTGCCAGCAGCCGCGGTAATACGTAGGTGGCAAGCGTTGTCCGGAATTATTGGGC

1

Species Identification Report

GTAAAGGGCTCGCAGGCGGTTTCTTAAGTCTGATGTGAAAGCCCCCGGCTCAACCGGGGAGGGTCATTGGAAACT
GGGGAACTTGAGTGCAGAAGAGGAGAGTGGAATTCCACGTGTAGCGGTGAAATGCGTAAAGATGTGGAGGAACAC
CAGTGGCGAAGGCGACTCTCTGGTCTGTAACTGACGCTAAGGAGCGAAAGCGTGGGAAGCGAACAGGATTAGATA
CCCTGGTAGTCCACGCCGTAAACGATGAGTGCTAAGTGTTAGGGGGTTTCCGCCCCTTAGTGATGCAGCTAACGC
ATTAAGCAGTCCGCCTGGGGAGTACGGTGGTAAGACTGAAAATTAAAGGAATTGATGGGGGCGCGCACAAGAGGT
GGAGCATGTGGTTTAATTCGAAGCAACGCGAAGAACCTTACCAGGTGTTGACGTCATCTGATAATACTAGAGATA
GGAGGTGGCGTTCGGGGGCAGAGTGACAGGTGGTGTATGGTTGTCGTCAGCTCGTGTCGTGAGATGTTGGGTTAA
GTATCGCAACGAGTGGAACCCTTGATGTTAGTTGCTAGCATTCAGTTGGGCACTCTAAGGTGACTGCCGGTGACA
AACCGGAGGAAGGTGGGGATGAGGTCAAATCATCATGCTCCTTATGACGTGGGGTACACACGTGTTACAATGGAG
AGAAGAAAGGGGAGCGAAACAGCGAGGTTAAGCCAATCCTACAAATATGTTTTCAGTTCGGATCGCAGTATGCAA
CTAGACTGCGTGAAGATGGAATAGCTAGTAATAGTGGATGAGCATGCCGCGGTGAATACGTTGCCGGGGGGTGTA
GACACCGCCGGTCACACCACGAGAGTTTGTAAGACCCGAAGTCGGTGAGGTAGCCTTTTAGGAGCCAGCCGCCGA
AGGTGGG

Fig. 3 16S rRNA contig sequence of the bacterial isolate used for Ag NP biosynthesis

Identified organism based on BLAST top hit: *Bacillus subtilis*

The BLAST Results shows 100% Query Coverage and 96.09% Identity with *Bacillus subtilis* strain CICC10076 16S ribosomal RNA gene, partial sequence.



select all 100 sequences selected — GenBank | Graphics | Distance tree of results | MSA Viewer

Description	Scientific Name	Max Score	Total Score	Query Cover	E value	Per. Ident	Acc. Len	Accession
Bacillus subtilis strain CICC10076 16S ribosomal RNA gene, partial sequence	Bacillus sub...	2335	2335	100%	0.0	96.09%	1496	AY917141.1
Bacterium 1-gw2-2 16S ribosomal RNA gene, partial sequence	bacterium 1...	2335	2335	100%	0.0	96.09%	1479	DQ990020.1
Bacillus subtilis strain BPRIST007 16S ribosomal RNA gene, partial sequence	Bacillus sub...	2335	2335	100%	0.0	96.09%	1491	JF414760.1
Bacillus subtilis subsp. subtilis strain CICC 10076 16S ribosomal RNA gene, partial s...	Bacillus sub...	2335	2335	100%	0.0	96.09%	1496	GQ375227.1
Bacillus subtilis strain BPRIST009 16S ribosomal RNA gene, partial sequence	Bacillus sub...	2335	2335	100%	0.0	96.09%	1484	JF414762.1
Bacillus sp. Ant-2b partial 16S rRNA gene, isolate Ant-2b	Bacillus sp. ...	2335	2335	100%	0.0	96.09%	1459	HF678932.2
Bacillus subtilis strain BPRIST008 16S ribosomal RNA gene, partial sequence	Bacillus sub...	2335	2335	100%	0.0	96.09%	1461	JF414761.1
Bacillus subtilis strain RH17 16S ribosomal RNA gene, partial sequence	Bacillus sub...	2333	2333	100%	0.0	96.15%	1492	OM996107.1

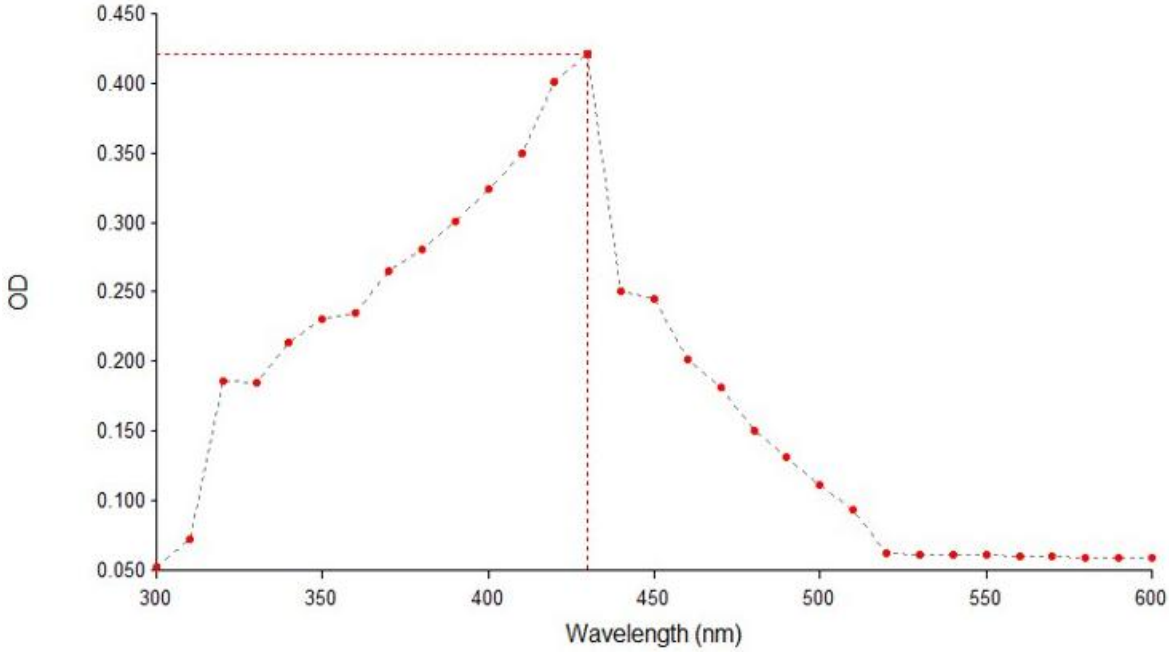
Fig.4 Summary of NCBI BLAST results for the 16S rRNA gene sequence of the bacterial isolate. The analysis identifies the organism as *Bacillus subtilis*, showing 100% query coverage and 96.09% sequence identity with strain CICC10076.

3.2 Characterization results of Ag NPs

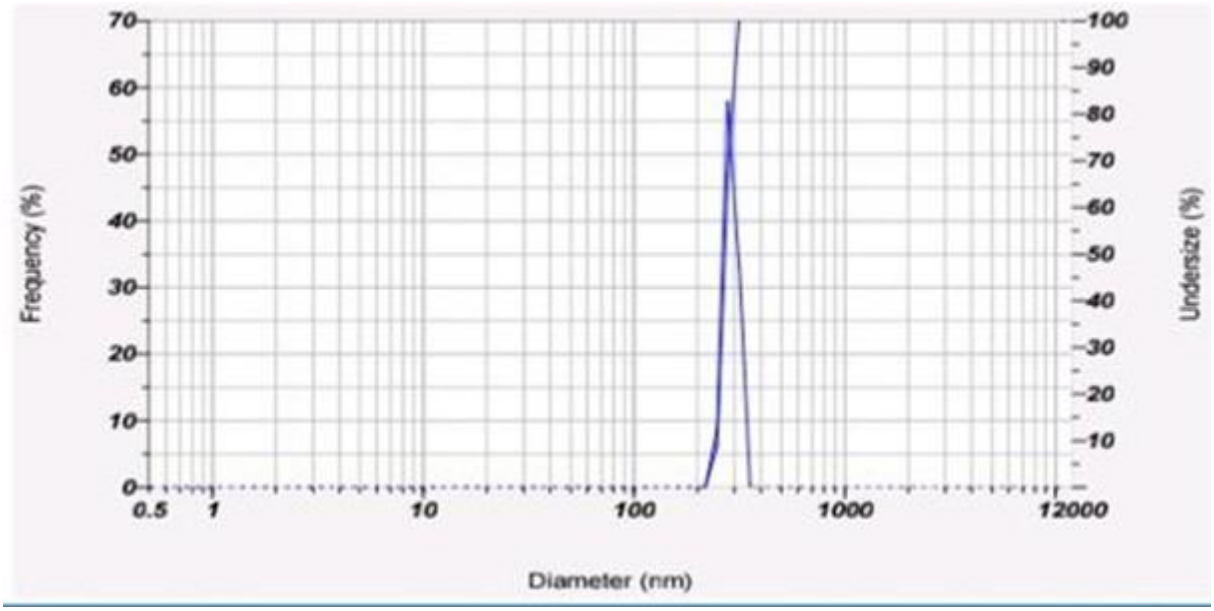
Change in the color of the reaction mixture from colorless solution to brown solution indicates the synthesis of silver nanoparticles [46]. The UV-Vis absorption spectra of the synthesized nanoparticles showed a characteristic Surface Plasmon Resonance (SPR) peak at 430 nm, confirming the successful formation of Ag NPs as shown in figure 5(a). The observed peak position is consistent with previously reported values for silver nanoparticles, further validating their synthesis. DLS analysis revealed that the biosynthesized Ag NPs displayed a hydrodynamic diameter of 271.3 ± 19.7 nm with a low PDI (0.0053), indicating a relatively uniform size distribution in suspension as shown in figure 5(b). The zeta potential was approximately 0 mV as shown in figure 5(c), reflecting an absence of measurable surface charge. The Ag NPs remained dispersed in the aqueous medium, highlighting that stability is rather provided by steric effects resulting from microbial capping biomolecules, even though such low values usually indicate minimal electrostatic stabilization. Microbial biosynthesis often results in nanoparticles coated with extracellular biomolecules such as proteins, enzymes, amino acids, and polysaccharides, which adsorb onto the nanoparticle surface and form a protective organic shell. This capping layer provides steric hindrance, preventing close approach and aggregation of particles by creating a physical barrier [47]. The combined DLS and zeta potential results therefore indicate that the colloidal stability of the synthesized Ag NPs is predominantly governed by biomolecule-mediated steric stabilization rather than electrostatic repulsion. Meanwhile, TEM images of the biosynthesized Ag NPs as shown in figure 5(d) and 5(e) revealed predominantly spherical nanoparticles forming densely aggregated clusters. This aggregation is likely due to drying effects during sample preparation, where particles lose their stabilizing solvent layer, combined with the near-zero zeta potential, which provides minimal electrostatic repulsion, reflecting the inherent tendency of the nanoparticles to agglomerate in the absence of charge-based stabilization [48]. Despite clustering, individual

primary nanoparticles could be resolved within the aggregates, and measurements of 100 discrete particles were found using ImageJ software and was used to generate a size distribution histogram using Origin software as shown in figure 5(f).

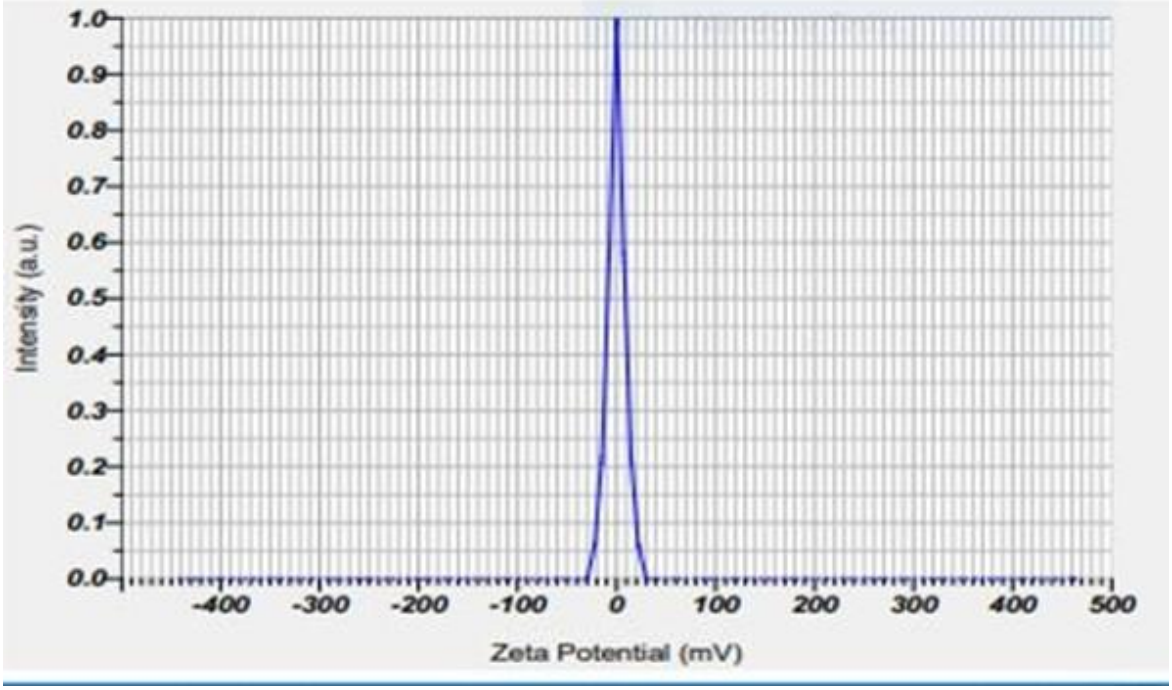
The average particle size was 62.5 ± 9.46 nm, indicating a relatively narrow distribution, consistent with DLS measurements in solution. Similar trend was observed in the previous study conducted by Ballotin et al., 2016 [48]. The zero-zeta potential suggests nearly zero electrostatic repulsion, so the clustering reflects the inherent tendency of the nanoparticles to agglomerate in the absence of charge-based stabilization. The corresponding SAED patterns displayed distinct concentric diffraction rings, corresponding to the (111), (200), (220), and (311) planes of face-centered cubic silver, confirming the crystalline nature of the nanoparticles as shown in figure 5(g) [49]. Together, these results indicate that the Ag NPs are stabilized in solution primarily through steric effects mediated by microbial biomolecules, which maintain colloidal dispersion despite the aggregation observed under TEM conditions. EDS analysis confirmed the elemental composition of the biosynthesized Ag NPs, with a strong and characteristic silver signal at ~3 keV, verifying the successful formation of silver nanoparticles [49]. Additional minor peaks corresponding to C, O, Fe, and Cl were also detected as shown in figure 5(h). The presence of carbon and oxygen is commonly associated with biomolecular capping agents originating from microbial metabolites, which enhance nanoparticle stability. Trace amounts of Fe and Cl may be derived from components of the culture medium or residual salts involved in the synthesis process. FTIR spectra revealed the functional groups involved in the reduction and stabilization of biosynthesized Ag NPs and displayed 5 distinct characteristic peaks as shown in figure 5(i). A broad absorption band at 3367 cm^{-1} corresponds to O–H and N–H stretching vibrations, indicative of hydroxyl and amine groups. The peak at 2087 cm^{-1} is attributed to N=C=S stretching, suggesting the presence of isothiocyanate groups. The peak at 1605 cm^{-1} corresponds to C=O stretching (amide I), while the band at 1063 cm^{-1} is associated with C=O stretching vibrations, typically from polysaccharides or alcohols. The signal at 836 cm^{-1} represents C–H bending, indicating aromatic compounds.


OD
0.450
0.400
0.350
0.300
0.250
0.200
0.150
0.100
0.050
300
350
400
450
500
550
600
Wavelength (nm)

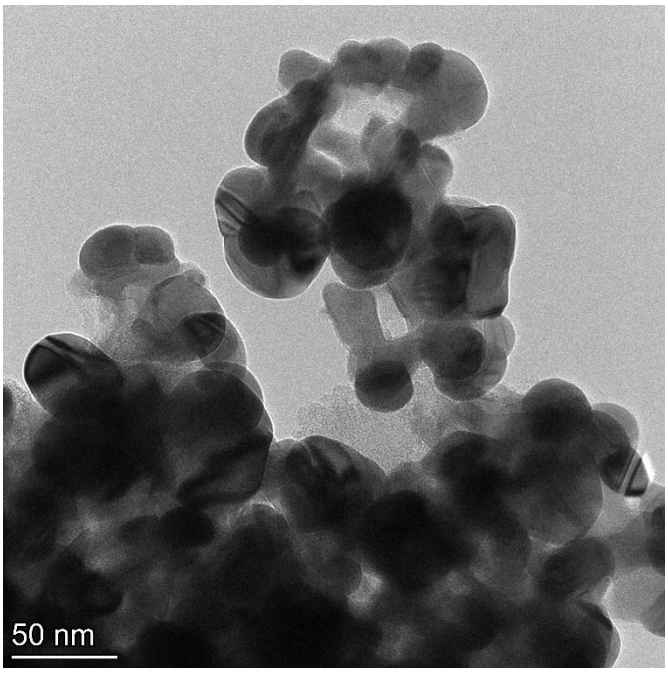
a)


Frequency (%)
70
60
50
40
30
20
10
0
0.5
1
10
100
1000
12000
Diameter (nm)
Undersize (%)
100
90
80
70
60
50
40
30
20
10

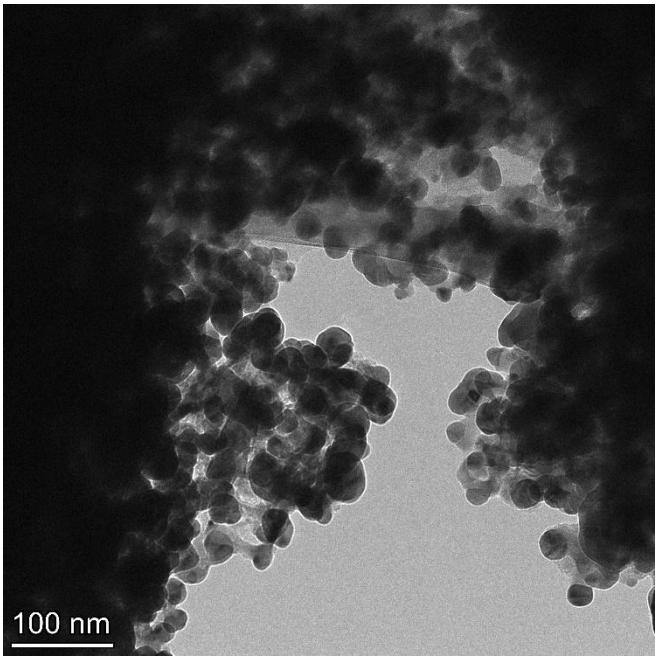
b)


Intensity (a.u.)
1.0
0.9
0.8
0.7
0.6
0.5
0.4
0.3
0.2
0.1
0.0
-400
-300
-200
-100
0
100
200
300
400
500
Zeta Potential (mV)

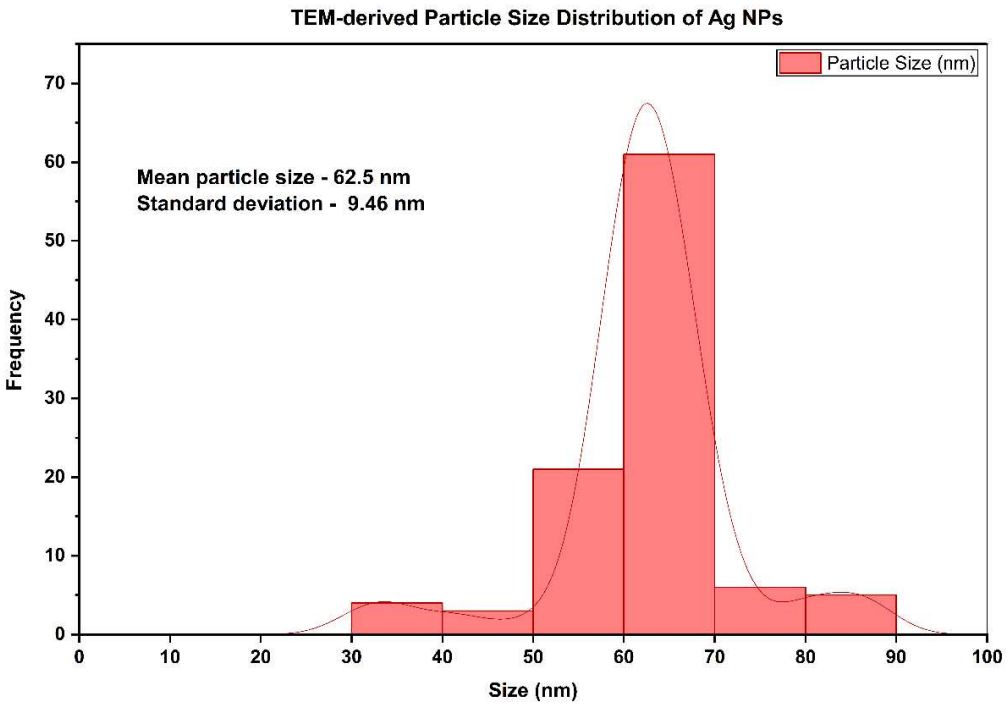
c)


50 nm

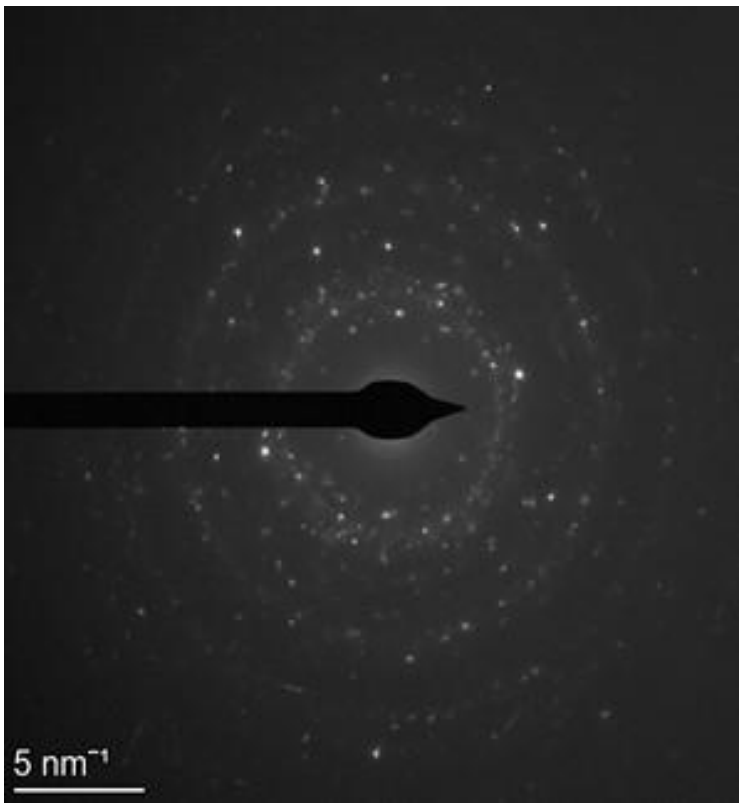
d)


100 nm

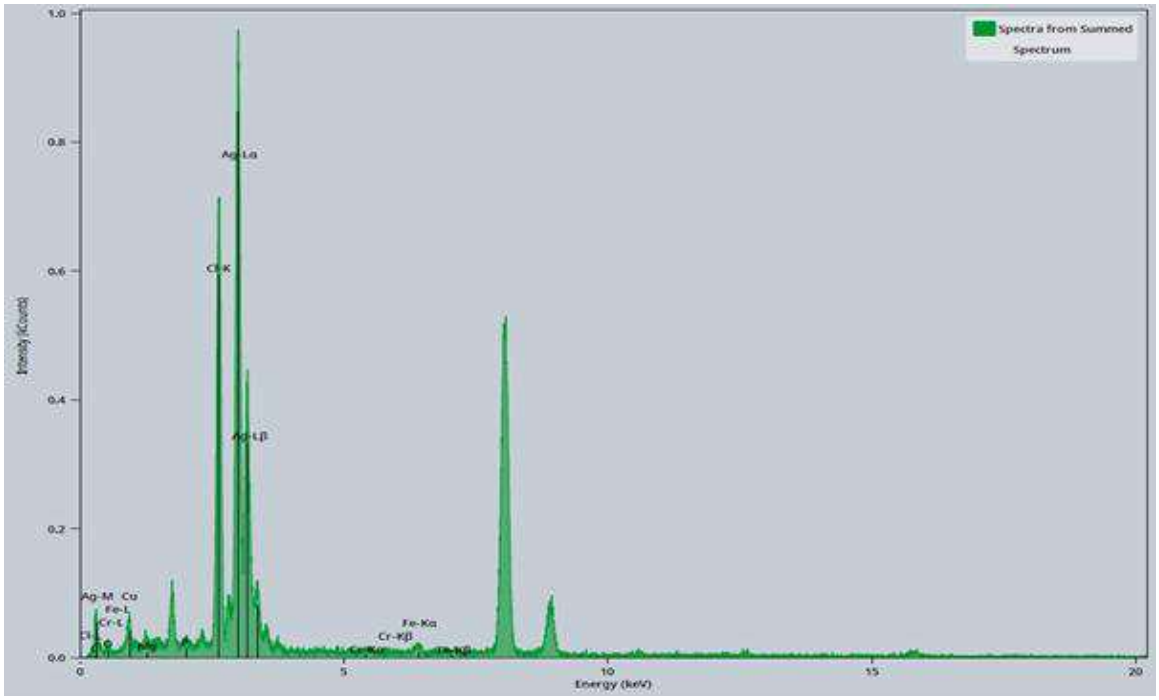
e)


TEM-derived Particle Size Distribution of Ag NPs
Particle Size (nm)
Mean particle size - 62.5 nm
Standard deviation - 9.46 nm
Frequency
Size (nm)
0
10
20
30
40
50
60
70
80
90
100

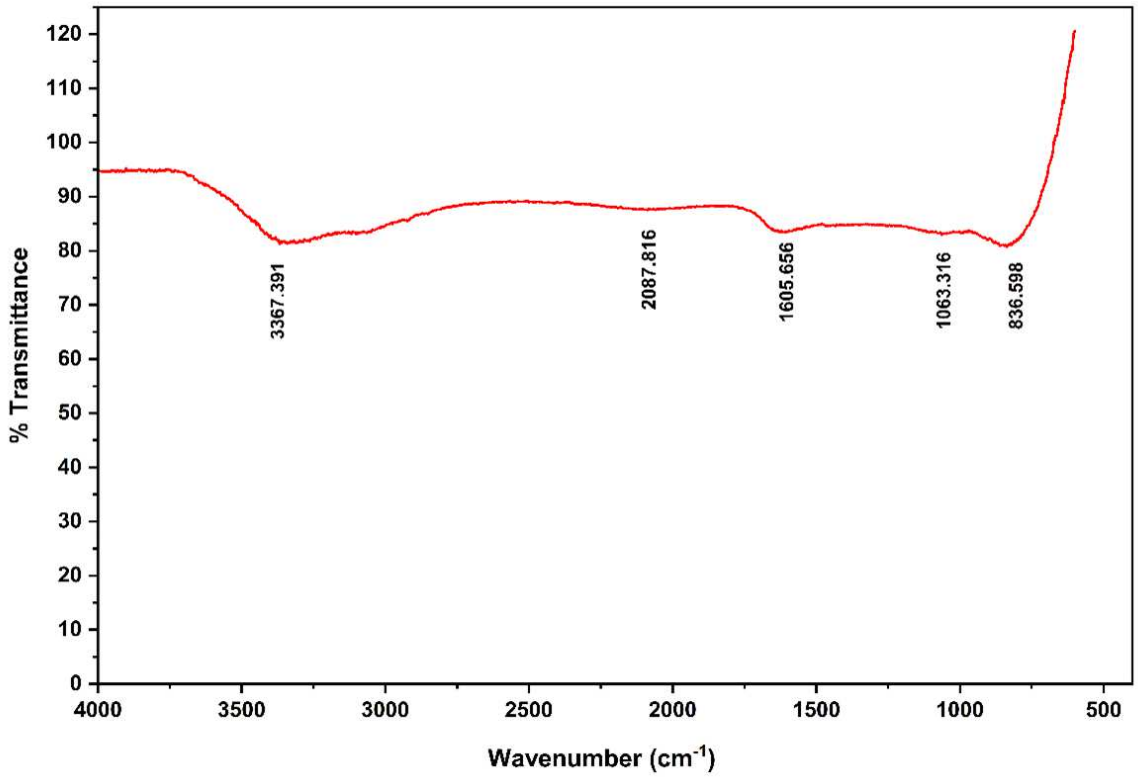
f)


5 nm⁻¹

g)


Spectra from Summed Spectrum
Ag-Lα
Cl-K
Ag-Lβ
Ag-M
Cu
Fe-L
Cr-L
Fe-Kα
Cr-Kβ
Intensity (kCounts)
Energy (keV)

h)


% Transmittance
Wavenumber (cm-1)
3367.391
2087.816
1605.656
1063.316
836.598

i)

Fig.5 Characterization profile of biogenic Ag NP synthesized using *Bacillus subtilis* AVK-21

(a) UV-Vis spectrum with SPR peak at 430 nm confirming Ag NP formation; (b) DLS hydrodynamic diameter distribution showing a mean diameter of 271.3 ± 19.7 nm and a low PDI = 0.0053, indicating uniform particle size in suspension; (c) Zeta potential curve showing a peak at 0 mV, indicating minimal surface charge and a tendency toward particle agglomeration ; (d) and (e) TEM image showing predominantly spherical nanoparticles; (f) SAED crystallographic ring pattern confirming the crystalline nature of the Ag NPs; (g) Particle size distribution histogram (n = 100) with mean particle diameter is 62.4 nm and standard deviation of 14.51 nm; (h) EDS spectrum with the strong signal at ~3keV confirming the elemental composition of silver; (i) FTIR spectrum showing characteristic absorption bands corresponding to functional groups

3.3 Congo red degradation results

The photocatalytic performance of the biosynthesized Ag NPs was assessed under UV and sunlight irradiation, and the degradation efficiency was quantified based on changes in absorbance at 497 nm over a period of 2 h.

Under UV light, the control showed negligible degradation of 3.22%, whereas the Ag NP-treated system achieved 37.8% degradation (Table 1). Visual observations confirmed progressive color fading in the Ag NP-treated sample as shown in figure 6. Compared to an rGO-Ag nanocomposite study that required hybrid materials to achieve comparable UV degradation [50], our pure Ag NPs exhibited efficient photodegradation, emphasizing the simplicity and green nature of the microbial synthesis route.

Under sunlight, the control exhibited minimal photolysis of 6.97%, while the Ag NPs achieved 67.02% degradation over 2 h (Table 2), nearly doubling the efficiency observed under UV and this can be seen in figure 7. This superior sunlight performance is attributed to the broader spectral range and higher photon flux, which enhances SPR excitation and ROS generation. In comparison, green-synthesized ZnO nanoparticles using gum arabic achieved 99.5% CR degradation in 30 min at pH 8 [51], magnetic $Mg_{0.5}Co_{0.5}Fe_2O_4$ spinel nanoparticles achieved 93% degradation under visible light [52] and myco-architectured CuO/Ag_2O-grafted graphene oxide nanoconjugate [53] achieved significant Congo Red degradation. While these systems demonstrate higher absolute efficiencies, they involve more complex synthesis and composition, our Ag NPs offer a simpler, microbially mediated approach that still achieves substantial degradation in 2 h.

Ag NPs synthesized from *Ocimum sanctum* reported high removal of Congo Red dye nearly 93% primarily through adsorption rather than photocatalysis [54]. In contrast, our study confirms that microbially synthesized Ag NPs not only remove Congo Red efficiently but also actively degrade it under light exposure, highlighting the dual role of biogenic capping biomolecules in stability and photocatalytic activity. While previous studies produced nanoparticles effective against Congo Red mainly through plant-mediated synthesis such as CuO-ZnO nanocomposite [55], Ag NP [56] [57], Ag-MgO nanoparticles [58], our study demonstrates that microbe-mediated synthesis of Ag NPs offers a greener, simpler, and single-component approach while achieving good photocatalytic degradation of Congo Red,

highlighting both efficiency and sustainability. Overall, these results demonstrate that sunlight drives significantly higher photocatalytic degradation than UV irradiation for microbially synthesized Ag NPs, and the simplicity, eco-friendliness, and single-component nature of this system offer a practical and sustainable alternative to more complex or chemically engineered nanomaterials reported in the literature.

Initial Absorbance = 0.373				
Time (min)	**Absorbance at 497 nm (Sample)**	**Degradation %**	**Absorbance at 497 nm (Control)**	**Degradation %**
15	0.344	7.77	0.371	0.54
30	0.32	14.21	0.37	0.80
45	0.315	15.55	0.369	1.07
60	0.281	24.66	0.368	1.34
90	0.255	31.64	0.365	2.14
120	0.232	37.8	0.361	3.22

Table.1 Time-dependent photodegradation of Congo Red under UV light in the presence of biosynthesized Ag NPs. Absorbance at 497 nm was measured at different time intervals, and the corresponding degradation percentages were calculated relative to the initial absorbance (0.373)

Initial Absorbance = 0.373				
Time (min)	**Absorbance at 497 nm (Sample)**	**Degradation %**	**Absorbance at 497 nm (Control)**	**Degradation %**
15	0.307	17.69	0.372	0.27
30	0.262	29.76	0.37	0.80
45	0.198	46.92	0.368	1.34
60	0.194	47.99	0.361	3.21
90	0.149	51.47	0.354	5.06
120	0.123	67.02	0.347	6.97

Table.2 Time-dependent photodegradation of Congo Red under sunlight in the presence of biosynthesized Ag NPs. Absorbance at 497 nm was recorded at different time intervals, and the corresponding degradation percentages were calculated relative to the initial absorbance (0.373)



a) b)

Fig.6 Photocatalytic degradation of Congo Red by biosynthesized Ag NPs under UV light. (a) Control and test flasks after 2 h of UV exposure. (b) Eppendorf tubes showing samples collected at different time intervals (0–120 min) from left to right, illustrating progressive dye degradation



a) b)

Fig.7 Photocatalytic degradation of dye by Ag NPs under sunlight **a)** Control and Test flask after 2 h under sunlight **b)** Eppendorf tubes containing test samples collected at various time intervals (from left to right) starting with the control sample and ending with the 120 min sample

A time-dependent comparison of dye degradation under UV and sunlight (Figure 8) further reveals that sunlight consistently produced higher efficiencies at all time points. At 15 min, degradation was approximately 10% under UV and 20% under sunlight, increasing progressively to nearly 30% and 70%, respectively, at 120 min. The superior sunlight-driven performance is attributed to enhanced SPR activation and more efficient charge separation under solar radiation. Overall, these findings confirm that microbially synthesized Ag NPs exhibit markedly enhanced photocatalytic activity under sunlight compared to UV irradiation. Their eco-friendly synthesis, single-component

nature, and effective photocatalytic action position them as a practical and sustainable material for dye degradation applications.

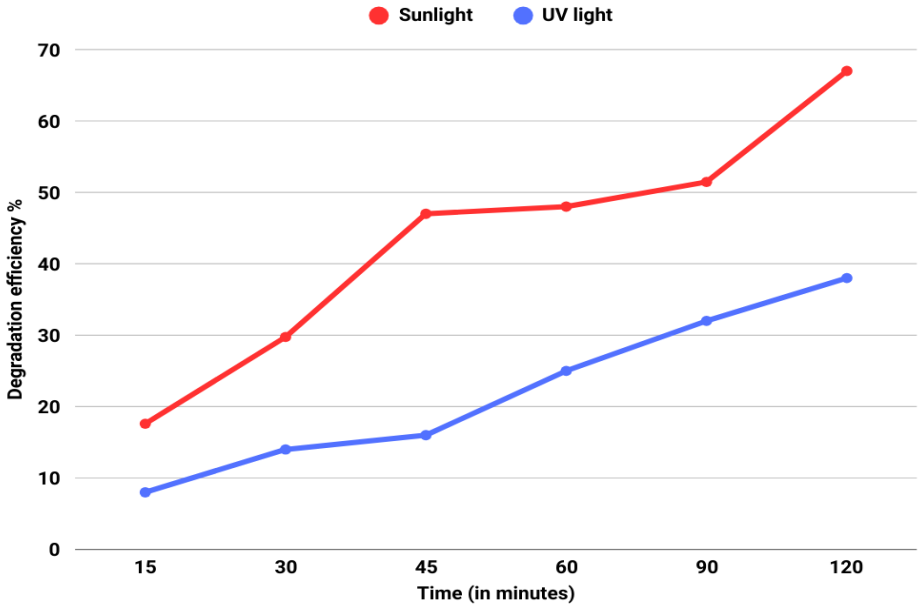


Fig.8 Comparison of degradation efficiency (%) of the synthesized Ag NPs under sunlight and UV light exposure over 120 minutes which shows sunlight exposure consistently yields a higher degradation efficiency than UV light

4. Conclusion

This study reports eco-friendly extracellular biosynthesis of silver nanoparticles (Ag NPs) using an isolated *Bacillus* subtilis *AVK-21* and a systematic evaluation of their physicochemical properties by various characterization techniques and photocatalytic performance. TEM analysis revealed that the biosynthesized Ag NPs were predominantly spherical with a primary particle diameter of 62.4 nm and a larger hydrodynamic diameter by DLS indicating agglomeration. EDS analysis confirmed the elemental composition of the nanoparticles showing the presence of silver. FTIR spectra showed functional groups present on Ag NPs which is contributed by microbial biomolecules that acted as reducing and capping agents, and SAED verified the face-centered cubic structure and crystallinity of the nanoparticle. The zeta potential result which was found to be 0.00 mV is consistent with the clustered morphology seen in TEM micrographs and explains the reduced electrostatic stabilization of the suspension. Functionally, the biosynthesized Ag NPs demonstrated significant photocatalytic activity against Congo Red. Under experimental condition, sunlight exposure achieved higher degradation than UV irradiation (67.0% under sunlight vs 37.8% under UV after 120 min), indicating that the broader solar spectrum and greater photon flux enhance SPR-mediated reactive species generation and catalytic efficiency for these biogenic Ag NPs. These results show that

microbially synthesized Ag NPs are promising, simple, and sustainable photocatalysts for dye remediation under natural sunlight. While previous studies conducted by Pathan et al., reported *B. subtilis*-mediated Ag NP synthesis, their characterization was limited to UV-Vis and SEM and they only tested dye degradation under unspecified illumination[40], whereas the present study provides a more comprehensive physicochemical evaluation (TEM, DLS, zeta potential, SAED, FTIR) and functional photocatalytic assessment under sunlight and UV, highlighting the novelty and practical relevance of the locally isolated water-derived strain AVK-21.

Although these results establish microbial Ag NPs as simple, sustainable, and effective photocatalysts for dye remediation under natural sunlight, several areas remain underexplored and present opportunities for future research. Detailed mechanistic and kinetic studies, including identification of reactive oxygen species, reaction pathways, and rate-law analysis under different illumination spectra, are necessary to fully understand the photocatalytic process. The performance of biosynthesized Ag NPs in real industrial effluents with complex matrices and competing ions remains largely untested, and systematic surface modification strategies to improve dispersion, stability, and catalytic surface area are rarely reported. Comprehensive environmental safety assessments, including ecotoxicity studies and life-cycle evaluations, are also limited, as are scale-up studies and pilot-scale deployment for practical wastewater treatment applications. Addressing these gaps will be critical to enhancing the stability, efficiency, and environmental compatibility of biogenic Ag NPs, ultimately facilitating their translation from laboratory-scale demonstrations to robust, field-ready solutions for sustainable wastewater remediation.

Data Availability:

The 16S rRNA sequence of Bacillus subtilis AVK-21 has been deposited in NCBI under the accession number PV663177.

Statements and Declarations

Conflict of Interest

The authors declare that they have no conflict of interest.

Funding

The authors did not receive support from any organization for the submitted work.

Competing interests

The authors have no relevant financial or non-financial interests to disclose.

Ethics Approval

Not applicable.

Consent to Participate

Not applicable.

References

1. S. Zafar, D. A. Bukhari, and A. Rehman, “Azo dyes degradation by microorganisms – An efficient and sustainable approach,” Saudi Journal of Biological Sciences, vol. 29, no. 12, p. 103437, Sep. 2022, doi: 10.1016/j.sjbs.2022.103437.
2. Oladoye, P. O., Bamigboye, M. O., Ogunbiyi, O. D., & Akano, M. T. (2022). Toxicity and decontamination strategies of Congo red dye. Groundwater for Sustainable Development, 19, 100844. https://doi.org/10.1016/j.gsd.2022.100844
3. Quintanilla-Villanueva, G. E., Sicardi-Segade, A., Luna-Moreno, D., Núñez-Salas, R. E., Villarreal-Chiu, J. F., & Rodríguez-Delgado, M. M. (2025). Recent Advances in Congo Red Degradation by TiO2-Based Photocatalysts Under Visible Light. Catalysts, 15(1), 84. https://doi.org/10.3390/catal15010084
4. Siddiqui, S. I., Allehyani, E. S., Al-Harbi, S. A., Hasan, Z., Abomuti, M. A., Rajor, H. K., & Oh, S. (2023). Investigation of Congo Red Toxicity towards Different Living Organisms: A Review. Processes, 11(3), 807. https://doi.org/10.3390/pr11030807
5. M. Kamali, F. Fazlpour, F. Karimi, A. Rezaee, F. Sadri, and S. F. Hosseini, “A review of cytotoxic effects of Azo dyes on brain-subregion,” Middle East Journal of Rehabilitation and Health Studies, vol. 10, no. 2, Feb. 2023, doi: 10.5812/mejrh-130751.
6. K. Meghwal, S. Kumawat, C. Ameta, and N. K. Jangid, “Effect of dyes on water chemistry, soil quality, and biological properties of water,” in Advances in human services and public health (AHSPH) book series, 2019, pp. 90–114. doi: 10.4018/978-1-7998-0311-9.ch005.
7. Y. Liu, C. Li, J. Bao, X. Wang, W. Yu, and L. Shao, “Degradation of Azo Dyes with Different Functional Groups in Simulated Wastewater by Electrocoagulation,” Water, vol. 14, no. 1, p. 123, Jan. 2022, doi: 10.3390/w14010123.
8. L. R. S. Pinheiro, D. G. Gradíssimo, L. P. Xavier, and A. V. Santos, “Degradation of azo dyes: Bacterial potential for bioremediation,” Sustainability, vol. 14, no. 3, p. 1510, Jan. 2022, doi: 10.3390/su14031510.
9. C. K. Githala, S. Raj, A. Dhaka, S. C. Mali, and R. Trivedi, “Phyto-fabrication of silver nanoparticles and their catalytic dye degradation and antifungal efficacy,” Frontiers in Chemistry, vol. 10, Sep. 2022, doi: 10.3389/fchem.2022.994721.
10. Abbas, R., Luo, J., Qi, X., Naz, A., Khan, I. A., Liu, H., Yu, S., & Wei, J. (2024). Silver Nanoparticles: Synthesis, Structure, Properties and Applications. Nanomaterials, 14(17), 1425. https://doi.org/10.3390/nano14171425
11. D. A. Patiño-Ruiz, S. I. Meramo-Hurtado, Á. D. González-Delgado, and A. Herrera, “Environmental Sustainability Evaluation of iron oxide nanoparticles synthesized via green synthesis and the coprecipitation Method: a Comparative Life cycle Assessment study,” ACS Omega, vol. 6, no. 19, pp. 12410–12423, May 2021, doi: 10.1021/acsomega.0c05246.

12. S. S. Salem and A. Fouda, “Green Synthesis of Metallic Nanoparticles and Their Prospective Biotechnological Applications: an Overview,” Biological Trace Element Research, vol. 199, no. 1, pp. 344–370, May 2020, doi: 10.1007/s12011-020-02138-3.
13. A.Fariq, T. Khan, and A. Yasmin, “Microbial synthesis of nanoparticles and their potential applications in biomedicine,” Journal of Applied Biomedicine, vol. 15, no. 4, pp. 241–248, Apr. 2017, doi: 10.1016/j.jab.2017.03.004.
14. P. Singh, Y.-J. Kim, D. Zhang, and D.-C. Yang, “Biological Synthesis of Nanoparticles from Plants and Microorganisms,” Trends in Biotechnology, vol. 34, no. 7, pp. 588–599, Mar. 2016, doi: 10.1016/j.tibtech.2016.02.006.
15. M. Saravanan, S. K. Barik, D. MubarakAli, P. Prakash, and A. Pugazhendhi, “Synthesis of silver nanoparticles from Bacillus brevis (NCIM 2533) and their antibacterial activity against pathogenic bacteria,” Microbial Pathogenesis, vol. 116, pp. 221–226, Jan. 2018, doi: 10.1016/j.micpath.2018.01.038.
16. B. Buszewski et al., “Antimicrobial activity of biosilver nanoparticles produced by a novel Streptacidiphilus durhamensis strain,” Journal of Microbiology Immunology and Infection, vol. 51, no. 1, pp. 45–54, Apr. 2016, doi: 10.1016/j.jmii.2016.03.002.
17. Z. Sanaeimehr, I. Javadi, and F. Namvar, “Antiangiogenic and antiapoptotic effects of green-synthesized zinc oxide nanoparticles using Sargassum muticum algae extraction,” Cancer Nanotechnology, vol. 9, no. 1, Mar. 2018, doi: 10.1186/s12645-018-0037-5.
18. S. R. Waghmare, M. N. Mulla, S. R. Marathe, and K. D. Sonawane, “Ecofriendly production of silver nanoparticles using Candida utilis and its mechanistic action against pathogenic microorganisms,” 3 Biotech, vol. 5, no. 1, pp. 33–38, Jan. 2014, doi: 10.1007/s13205-014-0196-y.
19. S. Saeed, A. Iqbal, and M. A. Ashraf, “Bacterial-mediated synthesis of silver nanoparticles and their significant effect against pathogens,” Environmental Science and Pollution Research, vol. 27, no. 30, pp. 37347–37356, Mar. 2020, doi: 10.1007/s11356-020-07610-0.
20. A.Deljou and S. Goudarzi, “Green Extracellular Synthesis of the Silver Nanoparticles Using Thermophilic Bacillus Sp. AZ1 and its Antimicrobial Activity Against Several Human Pathogenetic Bacteria,” Iranian Journal of Biotechnology, vol. 14, no. 2, pp. 25–32, Jun. 2016, doi: 10.15171/ijb.1259.
21. H. Sowani et al., “Green synthesis of gold and silver nanoparticles by an actinomycete Gordonia amicalis HS-11: Mechanistic aspects and biological application,” Process Biochemistry, vol. 51, no. 3, pp. 374–383, Dec. 2015, doi: 10.1016/j.procbio.2015.12.013.
22. N. Gürsoy, “Fungus-mediated synthesis of silver nanoparticles (Ag NP) and inhibitory effect on aspergillus spp. in combination with antifungal agent,” Cumhuriyet Science Journal, vol. 41, no. 1, pp. 311–318, Mar. 2020, doi: 10.17776/csj.653627.
23. N. Feroze, B. Arshad, M. Younas, M. I. Afridi, S. Saqib, and A. Ayaz, “Fungal mediated synthesis of silver nanoparticles and evaluation of antibacterial activity,” Microscopy Research and Technique, vol. 83, no. 1, pp. 72–80, Oct. 2019, doi: 10.1002/jemt.23390.

24. S. Zada et al., “Biogenic synthesis of silver nanoparticles using extracts of Leptolyngbya JSC-1 that induce apoptosis in HeLa cell line and exterminate pathogenic bacteria,” Artificial Cells Nanomedicine and Biotechnology, vol. 46, no. sup3, pp. 471–480, Sep. 2018, doi: 10.1080/21691401.2018.1499663.
25. D. Borah et al., “Alga-mediated facile green synthesis of silver nanoparticles: Photophysical, catalytic and antibacterial activity,” Applied Organometallic Chemistry, vol. 34, no. 5, Feb. 2020, doi: 10.1002/aoc.5597.
26. S. C. Paul et al., “Silver nanoparticles synthesis in a green approach: size dependent catalytic degradation of cationic and anionic dyes,” Oriental Journal of Chemistry, vol. 36, no. 03, pp. 353–360, Jun. 2020, doi: 10.13005/ojc/360301.
27. S. Jaast and A. Grewal, “Green synthesis of silver nanoparticles, characterization and evaluation of their photocatalytic dye degradation activity,” Current Research in Green and Sustainable Chemistry, vol. 4, p. 100195, Jan. 2021, doi: 10.1016/j.crgsc.2021.100195.
28. Kolya, H., Maiti, P., Pandey, A. et al. Green synthesis of silver nanoparticles with antimicrobial and azo dye (Congo red) degradation properties using Amaranthus gangeticus Linn leaf extract. J Anal Sci Technol 6, 33 (2015). https://doi.org/10.1186/s40543-015-0074-1
29. A. A. Lourthuraj, M. M. Selvam, M. S. Hussain, A.-W. A. Abdel-Warith, E. M. I. Younis, and N. A. Al-Asgah, “Dye degradation, antimicrobial and larvicidal activity of silver nanoparticles biosynthesized from Cleistanthus collinus,” Saudi Journal of Biological Sciences, vol. 27, no. 7, pp. 1753–1759, May 2020, doi: 10.1016/j.sjbs.2020.05.008.
30. B. Patel et al., “Bacteriogenic synthesis of morphologically diverse silver nanoparticles and their assessment for methyl orange dye removal and antimicrobial activity,” PeerJ, vol. 12, p. e17328, May 2024, doi: 10.7717/peerj.17328.
31. Okla, M.K., Javed, S., Tahir, M.F. et al. The Role of Silver Nanoparticles and Bacillus subtilis in Modulating Morpho–Physio–Biochemical Responses in Wheat (Triticum aestivum L.) Under Arsenic Stress. J Soil Sci Plant Nutr 25, 6294–6313 (2025). https://doi.org/10.1007/s42729-025-02531-8
32. Alfryyan, N., Kordy, M.G.M., Abdel-Gabbar, M. et al. Characterization of the biosynthesized intracellular and extracellular plasmonic silver nanoparticles using Bacillus cereus and their catalytic reduction of methylene blue. Sci Rep 12, 12495 (2022). https://doi.org/10.1038/s41598-022-16029-1
33. Z. H. Ali, L. Abdulazeem, W. A. Kadhim, M. H. Kzar, and O. J. Al-Sareji, “Application of green silver nanoparticles as anti-bacterial and photo-catalytic degradation of azo dye in wastewater,” Scientific Reports, vol. 14, no. 1, Dec. 2024, doi: 10.1038/s41598-024-76090-w.
34. Baird, R., & Bridgewater, L. (2017). Standard methods for the examination of water and wastewater. 23rd edition. Washington, D.C.: American Public Health Association.
35. Sanders E. R. (2012). Aseptic laboratory techniques: plating methods. Journal of visualized experiments : JoVE, (63), e3064. https://doi.org/10.3791/3064
36. Katz, D. S. (2008). The streak plate protocol. Microbe Library, 1-14.
37. Dettmeyer, R. B. (2018). Staining techniques and microscopy. In R. B. Dettmeyer (Ed.), Forensic histopathology: Fundamentals and perspectives (pp. 17–45). Cham: Springer International Publishing.

38. Janda JM, Abbott SL. 2007. 16S rRNA Gene Sequencing for Bacterial Identification in the Diagnostic Laboratory: Pluses, Perils, and Pitfalls. J Clin Microbiol 45. https://doi.org/10.1128/jcm.01228-07

39. Vimal, A., Aditya, S., & Kavipraba, A. (2025). Exploring microbial nanoparticle biosynthesis and its impact. Environmental Quality Management, 34(4). https://doi.org/10.1002/tqem.70093

40. Pathan, S., Wasnik, D. D., & Tumane, P. M. (2017). Comparative study of biodegradation of azo dyes from nanoparticles synthesized by using plant (Tridax procumbens) and bacteria (Bacillus subtilis). Asian Journal of Science and Technology, 8(8), 4740–4747.

41. Ali, S.A., Osman, M.E. & Mohamed, E.T. Eco-friendly biosynthesis of silver nanoparticles using marine-derived Fusarium exquisite: optimization, characterization, and evaluation of antimicrobial, antioxidant, and cytotoxic activities. World J Microbiol Biotechnol 41, 165 (2025). https://doi.org/10.1007/s11274-025-04368-w

42. Pasieczna-Patkowska, S., Cichy, M., & Flieger, J. (2025). Application of Fourier Transform Infrared (FTIR) Spectroscopy in Characterization of Green Synthesized Nanoparticles. Molecules, 30(3), 684. https://doi.org/10.3390/molecules30030684

43. Rajkumar, A., Sivarajasekar, N., & Kandasamy, S. (2021). Bio-Synthesized Silver Nanoparticles For Effective Photo- catalytic Degradation of Congo Red Dye in Aqueous Solutions: Optimization Studies Using Response Surface Methodology. Analytical Chemistry Letters, 11(6), 801–815. https://doi.org/10.1080/22297928.2021.1994007

44. Iwunze, M. O. (2010). Aqueous photophysical parameters of Congo Red. Spectroscopy Letters, 43(1), 16–21. https://doi.org/10.1080/00387010903278226

45. Gola, D., Kriti, A., Bhatt, N., Bajpai, M., Singh, A., Arya, A., Chauhan, N., Srivastava, S. K., Tyagi, P. K., & Agrawal, Y. (2021). Silver nanoparticles for enhanced dye degradation. Carbon Resources Conversion, 4, 100132. https://doi.org/10.1016/j.crgsc.2021.100132

46. Alruhaili, M.H., Selim, S., Adly, E. et al. Green synthesis of silver nanoparticles from Bacillus subtilis-mediated feather hydrolysate: antimicrobial, larvicidal against culex pipiens, and anticancer activities. Bioresour. Bioprocess. 12, 116 (2025). https://doi.org/10.1186/s40643-025-00952-y

47. Dawadi, Sonika, Katuwal, Saurav, Gupta, Aakash, Lamichhane, Uttam, Thapa, Ranjita, Jaisi, Shankar, Lamichhane, Ganesh, Bhattarai, Deval Prasad, Parajuli, Niranjan, Current Research on Silver Nanoparticles: Synthesis, Characterization, and Applications, Journal of Nanomaterials, 2021, 6687290, 23 pages, 2021. https://doi.org/10.1155/2021/6687290

48. Ballottin, D., Fulaz, S., Souza, M. L., Corio, P., Rodrigues, A. G., Souza, A. O., Gaspari, P. M., Gomes, A. F., Gozzo, F., & Tasic, L. (2016). Elucidating Protein Involvement in the Stabilization of the Biogenic Silver Nanoparticles. Nanoscale research letters, 11(1), 313. https://doi.org/10.1186/s11671-016-1538-y

49. Thirumagal, N., Jeyakumari, A.P. Photocatalytic and antibacterial activities of AgNPs from Mesua Ferrea seed. SN Appl. Sci. 2, 2064 (2020). https://doi.org/10.1007/s42452-020-03650-w

50. Ali, M.H.H., Goher, M.E., Al-Afify, A.D.G. et al. A facile method for synthesis rGO/Ag nanocomposite and its uses for enhancing photocatalytic degradation of Congo red dye. SN Appl. Sci. 4, 276 (2022). https://doi.org/10.1007/s42452-022-05163-0

51. Alhasan, H. S., Omran, A. R., Al Mahmud, A., Mady, A. H., & Thalji, M. R. (2024). Toxic Congo Red Dye Photodegradation Employing Green Synthesis of Zinc Oxide Nanoparticles Using Gum Arabic. Water, 16(15), 2202. https://doi.org/10.3390/w16152202

52. Harki, D. A. H., Naghipour, A., & Fardood, S. T. (2024). Eco-friendly synthesis and characterization of $Mg_{0.5}Co_{0.5}Fe_2O_4$ magnetic nanoparticles for photocatalytic degradation of Congo Red dye. Case Studies in Chemical and Environmental Engineering, 10, 101016. https://doi.org/10.1016/j.cscee.2024.101016

53. Omran, B. A., Abdel-Salam, M. O., Farghal, H. H., El-Sayed, M. M. H., & Baek, K.-H. (2025). Myco-architecture of proficient antibacterial CuO/Ag_2O-grafted graphene oxide nanoconjugates: Characterization and Congo Red degradation-assisted by the activation of peroxymonosulfate. Materials Research Bulletin. https://doi.org/10.1016/j.materresbull.2025.113496

54. Murugeshwari, S., Rathi, B. S., Kalaiarasi, N., Kumar, R. M. S., Arunkumar, I., Vasanth, M., Kumar, P. S., & Rangasamy, G. (2025). Green synthesis of silver nanoparticles using Ocimum sanctum for efficient Congo red dye removal: a response surface methodology approach. Environmental monitoring and assessment, 197(10), 1105. https://doi.org/10.1007/s10661-025-14525-1

55. Bopape, D. A., & Hintsho-Mbita, N. C. (2025). Commelina benghalensis-mediated CuO–ZnO nanocomposite: Effect of the p-n heterojunction on the photocatalytic activity against Congo Red and carbamazepine. Inorganic Chemistry Communications, 178, Article 114529. https://doi.org/10.1016/j.inoche.2025.114529

56. Albeladi, S. S. R., Malik, M. A., & Al-Thabaiti, S. A. (2020). Facile biofabrication of silver nanoparticles using Salvia officinalis leaf extract and its catalytic activity towards Congo red dye degradation. Journal of Materials Research and Technology, 9(5), 11088–11096. https://doi.org/10.1016/j.jmrt.2020.06.074

57. Shaikh, W. A., Chakraborty, S., & Islam, R. U. (2018). UV-assisted photo-catalytic degradation of anionic dye (Congo Red) using biosynthesized silver nanoparticles: a green catalysis. Desalination and Water Treatment, 110, 294–303. https://doi.org/10.5004/dwt.2018.23004

58. Benisha, R., Amalanathan, M., Aravind, M., Mary, M. S. M., Ahmad, A., Tabassum, S., Al-Qahtani, W. H., & Ahmad, I. (2022). Catharanthus roseus leaf extract mediated Ag–MgO nanocatalyst for photocatalytic degradation of Congo Red dye and their antibacterial activity. Journal of Molecular Structure, 133005. https://doi.org/10.1016/j.molstruc.2022.133005

Supplementary Files

This is a list of supplementary files associated with this preprint. Click to download.

- OnlineResource2.docx